

# Joint2Human: High-quality 3D Human Generation via Compact Spherical Embedding of 3D Joints

Muxin Zhang<sup>1,†</sup>, Qiao Feng<sup>1,†</sup>, Zhuo Su<sup>2</sup>, Chao Wen<sup>2</sup>, Zhou Xue<sup>2</sup>, Kun Li<sup>1,\*</sup>  
<sup>1</sup>College of Intelligence and Computing, Tianjin University  
<sup>2</sup>PICO IDL, ByteDance

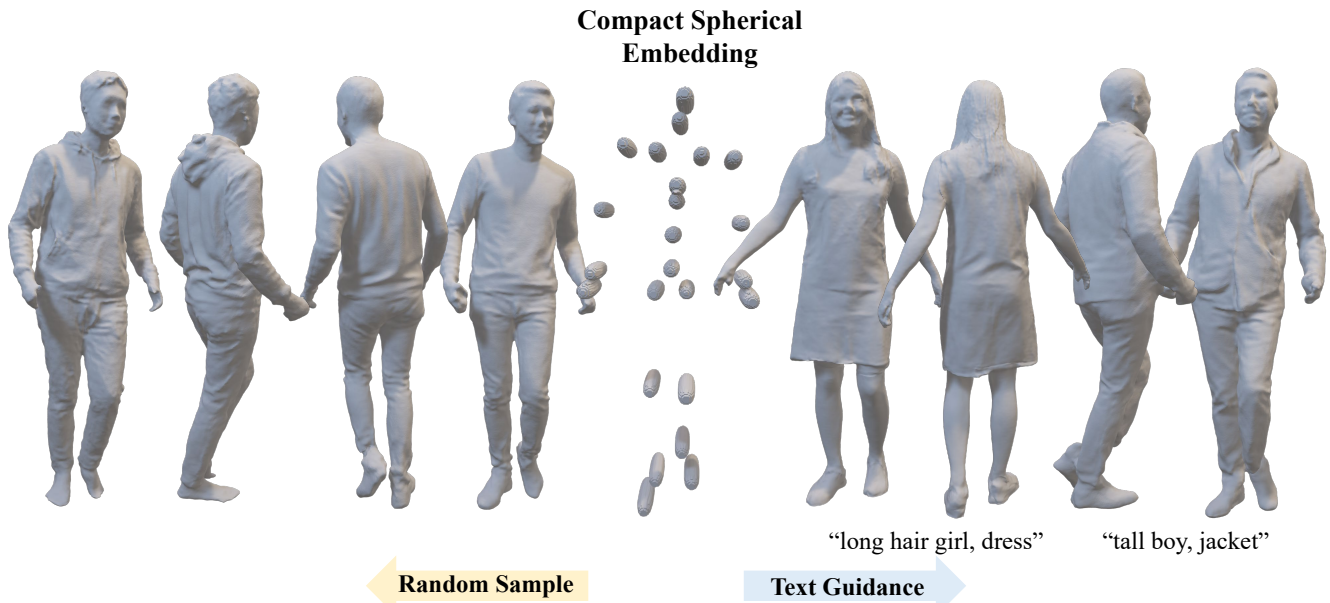


Figure 1. Our method can generate high-quality and high-resolution 3D humans with reasonable global structure and fine-grained geometry details in an efficient way, based on our proposed compact spherical embedding of 3D joints and a direct conditional 3D generative network with 2D diffusion models.

## Abstract

3D human generation is increasingly significant in various applications. However, the direct use of 2D generative methods in 3D generation often results in significant loss of local details, while methods that reconstruct geometry from generated images struggle with global view consistency. In this work, we introduce Joint2Human, a novel method that leverages 2D diffusion models to generate detailed 3D human geometry directly, ensuring both global structure and local details. To achieve this, we employ the Fourier occupancy field (FOF) representation, enabling the direct production of 3D shapes as preliminary results using 2D generative models. With the proposed high-

frequency enhancer and the multi-view recarving strategy, our method can seamlessly integrate the details from different views into a uniform global shape. To better utilize the 3D human prior and enhance control over the generated geometry, we introduce a compact spherical embedding of 3D joints. This allows for effective application of pose guidance during the generation process. Additionally, our method is capable of generating 3D humans guided by textual inputs. Our experimental results demonstrate the capability of our method to ensure global structure, local details, high resolution, and low computational cost, simultaneously. More results and code can be found on our project page at <http://cic.tju.edu.cn/faculty/likun/projects/Joint2Human>.

<sup>†</sup> Equal contribution.

\* Corresponding author.

## 1. Introduction

The field of 3D human generation holds considerable significance across diverse applications, including virtual/augmented reality, gaming, and the film industry. Despite advancements in existing methods [9, 21, 44], achieving a simultaneous guarantee of both global structural accuracy and preservation of local details remains a challenge, often compounded by high computational costs. In this paper, we aim to address these limitations and propose a methodology for generating high-quality 3D human models that exhibit fidelity to both global structures and local details, while ensuring computational efficiency, as illustrated in Figure 1.

Existing human generation methods can be divided into two categories: two-step generation methods and direct 3D generation methods. Two-step generation methods [18, 19, 21, 32, 44] generate 3D humans from 2D images via Nerf [28] or differentiable rendering [29]. These methods are trained only on 2D datasets and hence lack the perception of 3D global structures, which results in view inconsistency. Chupa [21] aims to produce high-quality results through dual normal map-based optimization but suffers from depth ambiguity issues that harm view consistency. Direct 3D generation methods [1, 9, 31, 42] generate 3D humans directly with Tri-planes [4] or Signed Distance Fields [32]. However, these approaches encounter challenges in achieving high-fidelity global structure with fine-grained local geometry details. Additionally, their generalization capabilities are limited, and computational efficiency is compromised. In summation, the existing methodologies collectively fall short in simultaneously ensuring global structural fidelity, local detail preservation, high resolution, and computational efficiency.

To achieve efficiently generating high-quality 3D humans with reasonable global structure and fine-grained geometry details, in this paper, we propose *Joint2Human*, a conditional generative network with 2D diffusion models derived from 3D datasets. To achieve high-fidelity 3D human generation with reasonable global structure, we employ an image-aligned 3D representation FOF to directly produce 3D shapes as preliminary results with 2D generative models. Additionally, we propose a compact spherical embedding of 3D joints for effective pose guidance, enhancing the overall fidelity of generated poses. We also design a high-frequency enhancer and a multi-view recarving strategy for fine-grained local detail generation. Experimental results demonstrate that our method outperforms the state-of-the-art methods in terms of global structure, local detail, and efficiency. Furthermore, our method also exhibits versatility by enabling the generation of 3D human representations guided by text.

To summarize, our main contributions include:

- We propose *Joint2Human*, a direct conditional 3D gen-

erative method with 2D diffusion model for high-quality, high-resolution 3D human generation. To our best knowledge, our work is the first work that can ensure global structure, local details, high resolution, and low computational cost, simultaneously.

- We propose a new 3D pose representation, a compact spherical embedding of 3D human joints, for efficient perception of global structure. This mechanism also facilitates a more straightforward and effective implementation of pose-guided generation.
- We design a high-frequency enhancer by integrating a subsidiary decoder into the pre-trained VAE, and a multi-view recarving strategy, for fine-grained local detail generation.

## 2. Related Work

### 2.1. 3D Human Generation with 2D Generators

Many approaches [11, 18, 19, 21, 32, 44] try to learn the 3D shape from 2D images via various Nerf representations [23, 25, 28, 30, 35, 36] and differentiable volume rendering [29, 43, 48]. It is always computationally expensive and limited in resolution. EVA3d [18] is carefully designed in terms of training strategy although it achieves high-resolution generation. What’s worse, the 2D dataset is always imbalanced in viewing angles and human poses, so this strategy is relatively unstable and hard to generate a realistic full-body human geometry. Other methods [19, 21, 44] also seek help with priors from 2D human generation and 3D human reconstruction models, which is cumbersome. In Chupa [21], many optimizations are needed to maintain viewpoint consistency. It first generates two normal maps for the front and back sides of a clothed human, then optimizes the 3D generated mesh by the dual normal maps. There are also some human template-based works [3, 17, 21, 45, 47] that are highly dependent on human template mesh, such as SMPL [26] and SMPL-X [34], which adversely affect the diversity of generated models especially in local details. For example, it is flawed in modeling loose clothes like dresses.

### 2.2. 3D-aware Generation

Based on the development of 3D human representation, numerous methods have emerged for direct 3D generation. Some of these approaches [1, 9, 31, 42] utilize tri-planes [4] which is a Nerf-based representation. It is hard to generate the precise geometry limited by the computational complexity. Apart from that, the implicit functions like SDFs [32, 33] are highly favored in several methods [3, 17, 18, 22, 44]. Alternatively, some methods use 3D data for training, gDNA [6] use implicit multi-subject forward skinning which enables learning from 3D scans of human bodies. Among all the works mentioned above, the

Table 1. Comparison with existing methods.

Method	Global Structure (View Consistency)	Local Detail	High Resolution	Loose Clothes	Computational Efficiency
GNARF[1]	✓	✗	✗	✗	✗
AG3D [9]	✓	✗	✗	✗	✗
Get3Dhuman [44]	✗	✓	✓	✓	✗
Chupa [21]	✗	✓	✓	✗	✗
<b>Ours</b>	✓	✓	✓	✓	✓

GAN [1, 4, 9, 12, 18, 19, 31, 32, 44, 47] and Diffusion models [3, 16, 21, 22, 42] are the most popular. There are also some human template-based works [3, 17, 21, 45, 47] that are highly dependent on human template mesh, such as SMPL [26] and SMPL-X [34], which adversely affect the diversity of generated models especially in local details. For example, it is flawed in modeling loose clothes like dresses.

Using the diffusion model for small object generation[5, 7, 8, 24] is easier to combine with text control. However, the text-guided 3D human generation is more difficult due to the high-dimensional cube and lack of text-3D data pairs. In such a situation, some attempts were made. Avatar-CLIP [17] initialize a bare mesh shape with SMPL, then it continuously optimizes the mesh to match the input text by calculating the CLIP score between the text token and the rendering image of mesh, CLIP-actor [45] does the same thing except it designs a recommendation module to get the initial shape/motion. In this way, they reduced the need for text-3D data pairs with the help of the large text-image pre-trained model [37]. Other methods [3, 21, 42] impose textual controls on the diffusion model for generated shapes that match the input description.

Different from the two types of methods described above, as shown in Tab. 1. Our approach can accommodate both global structures and local details. To fully perceive the global structures, we adopt the image-aligned 3D representation FOF and introduce a compact spherical embedding of 3D joints for pose guidance. To generate details, we design a high-frequency enhancer and a multi-view recarving strategy in 3D space. Apart from this, we also simultaneously achieve high-resolution generation and low computational cost.

### 3. Preliminaries

#### 3.1. Fourier Occupancy Fields

Fourier Occupancy Field (FOF) [10] is an efficient 3D representation based on the Fourier series expansion of a square-wavelike function. It spans the 3D occupancy field along the view direction and takes the low frequency terms to represent the human geometry with a 2D map. This can

be written as:

$$F(x, y, z) = b^T(z)C(x, y), \quad (1)$$

where  $b^T(\cdot)$  is the basic functions, and  $C(\cdot, \cdot)$  is the FOF. Such a representation enables direct inference of 3D geometry using 2D frameworks. Thanks to the convenient conversion between the FOF and 3D occupancy field, we can integrate the details from different views into a uniform 3D field with our multi-view recarving strategy, which is described in Sec. 4.3.

#### 3.2. Diffusion Probabilistic Model

Diffusion Probabilistic Models [16] is a generative model that could realize high-quality image generation. It contains two processes, the fixed forward process  $q$  and backward processes  $p$  which can be viewed as a Markov chain indexed by timestep  $t$ . In the forward process, we gradually add Gaussian noise  $\epsilon$  to raw datapoint  $z_0$  in each timestep  $t$ , we have:

$$z_t = \sqrt{\bar{\alpha}_t}z_0 + \sqrt{1 - \bar{\alpha}_t}\epsilon, \quad (2)$$

where we use a sequence of increasing noise schedules  $\beta_t \in \{\beta_1, \dots, \beta_T\}$  with the last timestep  $T$ ,  $\alpha_t = 1 - \beta_t$  and  $\bar{\alpha}_t = \prod_{s=1}^t \alpha_s$ . After sufficient noising steps, the raw data  $z_0$  is transformed to pure Gaussian noise. Then it's time for the backward process  $p$ , which adopts a U-Net [39] structure as the denoising model  $\epsilon_\theta$ , trained to predict the noise added at every step for removing noise. The loss functions can be expressed simply in the form of:

$$\mathcal{L}_{DDPM}(\theta) := \mathbb{E}_{\mathbf{z}, \epsilon \sim N(0,1), t} \left[ \|\epsilon - \epsilon_\theta(\mathbf{z}_t, t)\|^2 \right]. \quad (3)$$

For generation, we first sample a noise  $z_t \sim N(0, 1)$  from the Gaussian distribution during inference time. Then we gradually denoise  $z_t$  step by step by estimating  $\epsilon$ . The reverse process can be formulated as:

$$\mu_\theta(z_{t-1}, t) = \frac{1}{\sqrt{\alpha_t}} \left( z_t - \frac{\beta_t}{\sqrt{1 - \bar{\alpha}_t}} \epsilon_\theta(z_t, t) \right). \quad (4)$$

We can obtain the final results by iteratively computing  $z_{t-1} = \mu_\theta(z_{t-1}, t) + \sigma_t \epsilon$  along with the denoising process.

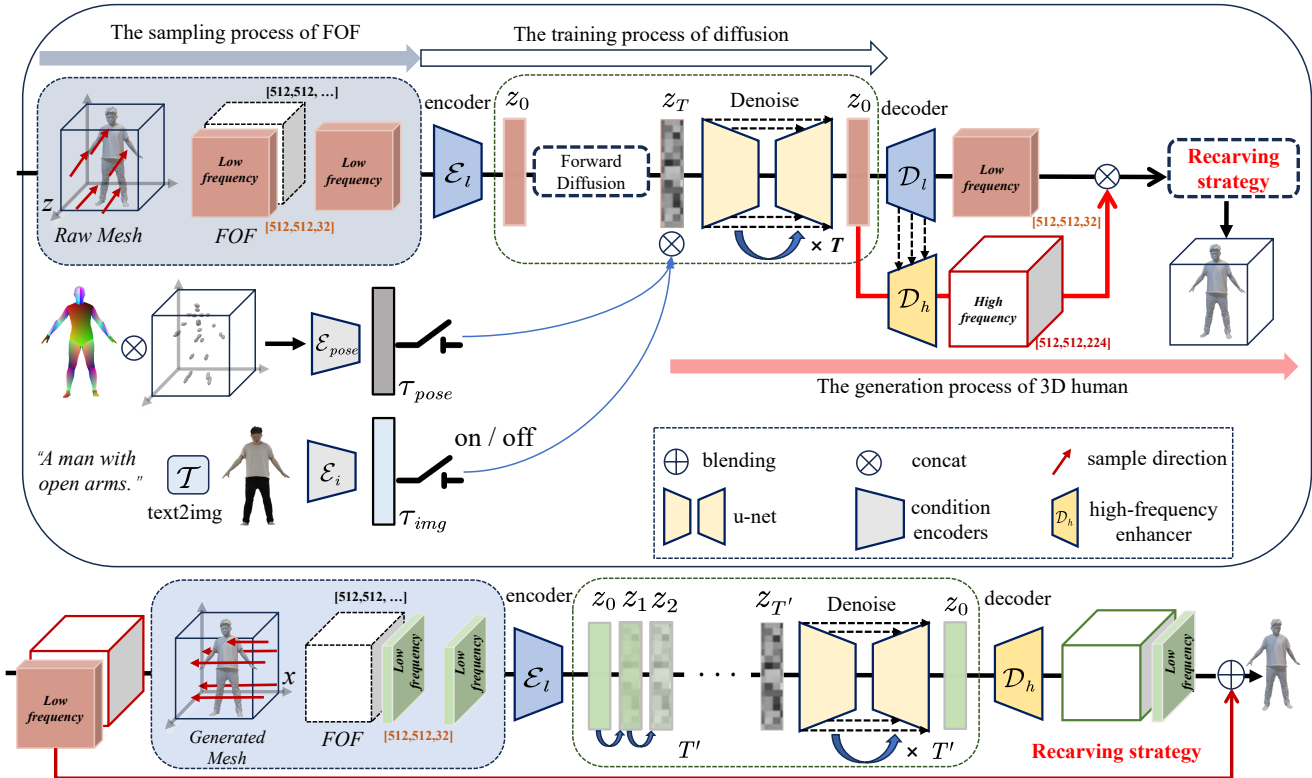


Figure 2. **Overview of our framework.** *Joint2Human* takes gaussian noise and some conditional information (pose, text) as input. To enable high-resolution human generation, we first encode FOF into a latent space, where a diffusion model is trained. Furthermore, to enable flexible conditional generation, we adopt condition encoders along with classifier-free guidance to enable conditional generation. Our conditional control generation strategy can support switching between different modalities. Then, we pass the results generated by the first denoising process through the high-frequency enhancer  $\mathcal{D}_h$  and multi-view recarving strategy for fine-grained local detail generation. Additionally, the recarving strategy is shown in the bottom subfigure.

## 4. Method

Our work aims at generating 3D full-body human models with global structure and local details. To achieve this, we design an effective pipeline as illustrated in Fig. 2. The highlight of our work is that we propose a direct conditional 3D generative method with 2D diffusion models. Specifically, we use an image-aligned 3D representation FOF [10] to directly produce 3D shapes. Then, we model the distribution of FOF features. However, the raw data space is high-dimensional and high-resolution, so modeling these feature maps is too costly to compute. So, we first map Fourier Occupancy Fields to a low dimensional space and then operate our condition and generation process in the latent space (Sec. 4.1). For reasonable global structure and effective pose guidance, we propose a compact spherical embedding of the 3D human joints (Sec. 4.2). Furthermore, We also design a high-frequency enhancer (Sec. 4.3) and a multi-view recarving strategy (Sec. 4.4) for fine-grained local detail generation. We will detail all the stages of our method in the following subsections.

### 4.1. Latent Diffusion for Fourier Occupancy Fields

To model the distribution of Fourier Occupancy Fields, following the latent diffusion model [38], we utilize an auto-encoder to compress the high-dimensional raw data space into a lower-dimensional latent space, which encodes each shape into a normal distribution. In detail, we adopted a VAE-like auto-encoder which contains the encoder  $\mathcal{E}$  and decoder  $\mathcal{D}$ . Given a FOF feature  $x \in \mathbb{R}^{512 \times 512 \times 32}$ , the encoder  $\mathcal{E}$  encodes FOF into latent vectors  $z = \mathcal{E}(x)$ , where  $z \in \mathbb{R}^{128 \times 128 \times 8}$ . The decoder  $\mathcal{D}$  decodes the latent vectors back to the original FOF space  $\hat{x} = \mathcal{D}(z)$ , where  $\hat{x} \in \mathbb{R}^{512 \times 512 \times 32}$ . We pretrained the auto-encoder with the reconstruction loss and KL-regularization loss. Before DDPM model training, we freeze the weights of the VAE, and the training data is passed through the encoder  $\mathcal{E}$  in the vae module to obtain its feature in the latent space. We adopt a U-Net-like structure as our denoising model  $\epsilon_\theta$ . We follow the classical and efficient loss function proposed by Ho [16] and train the diffusion model based on the feature from noise with the diffusion model in the latent

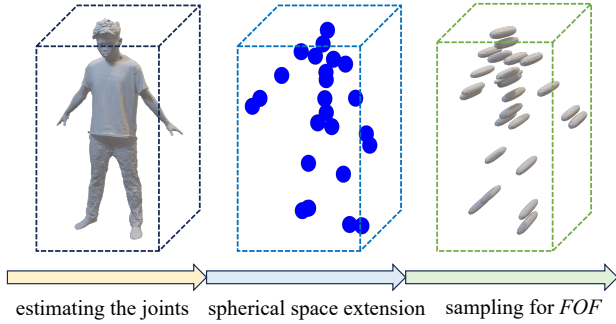


Figure 3. The generation process for compact spherical embedding of 3D joints. Given a human mesh, we first compute its 3D joint points. Then we generate a solid ball around each joint and convert them to FOF. For the compact spherical embedding of 3D joints, we only retained the low-frequency information, so the visualization results are not strictly spherical.

space. Thus we can obtain a vector  $\tilde{z}_0$  in the latent space, which will be sent to the decoder  $\mathcal{D}$  to get Fourier occupancy fields. Then, we can get the 3D occupancy field from FOF. We can get the 3D human mesh from the 3D occupancy field with the Marching Cubes [27] algorithm. In this way, we have further mitigated the computational cost of 3D representations.

## 4.2. Condition-guided Generation Mechanisms

**Compact Spherical Embedding of 3D Joints.** Instead of adopting the pose-guidance from the human parametric models [26, 34]. Many previous works [3, 9, 17, 21, 45, 47] rely on SMPL or SMPL-X as pose guidances, which adversely affects the diversity of generated models especially in local details. Regardless of whether SMPL mesh or a normal map from SMPL is used as the reference to generate a clothed human body, this information from the strong geometric prior is redundant. Thus, our model may be misleading to learn the extra knowledge. As a result, it may memorize the training set during training. Even during inference, the generated result closely resembles the highly desired results from the training set. To avoid denoising model  $\epsilon_\theta$  from being in an over-fitting regime, we propose compact spherical embedding for 3D human joints, encompassing both the 2D position and depth in 3D space as shown in Fig. 3 we only save the  $K$  joints location  $J = \{p_i \in \mathbb{R}^3\}_{i=1}^K$  from the whole human body as our guidance. For each joint position  $p_i$ , We extend a solid sphere with  $p_i$  as the center and  $r$  as the radius in 3D space. After that, according to the Sec. 3.1, we compute the FOF  $C_i \in \mathbb{R}^{512 \times 512 \times 8}$  of each solid sphere. Then we concat  $\{C_i\}_{i=1}^K$  channel-wise as our joint condition  $con_{joint} \in \mathbb{R}^{512 \times 512 \times 8K}$ . During training, we apply the joint condition  $con_{joint}$  on the latent code  $z$  after passing

through the conditional encoder.

**Pose-guided Geometry Generation.** Given a 3D human pose, our goal is to generate a human body shape that fits the given pose. With the compact spherical embedding of the 3D joints, we can efficiently perform pose control of human generation. After observing the generated results, we found that we occasionally encountered the issue of inconsistent orientation between the upper and lower halves of the generated human. To address it, we incorporate 2D prior information by utilizing the IUUV map as defined in DensePose [13]. In the training stage, we learn a pose encoder to get the human pose embedding  $\tau_{pose}$ , then apply it to the training of the diffusion model. In the inference stage, we first get the human pose embedding  $\tau_{pose}$  from the input pose priori, then we perform the denoising process of the  $\epsilon_\theta$  to get a 3D human shape.

**Text-guided Geometry Generation.** Given a textual description, our goal is to generate a 3D human that fits the text input. Previous methods often rely on the CLIP model to extract the embeddings from text and images, these features play an important role in the process of training and testing. However, this strategy depends on the textual annotation of the training data that is missing for us.

To generate the 3D human with the guidance of text description, we proposed the image prompt strategy for our model based on a text-guided 2D human image generation model Text2Human [20]. In the training stage, We learn an additional image encoder to get the human image embedding  $\tau_{img}$ , then apply it to the training of the diffusion model. In the inference stage, with the input text, we first infer the text-to-image model  $\mathcal{T}$  to get the human image  $I_h$ , then we sample the 3D human shape from  $\epsilon_\theta$ . We provide additional text-guided generation results in the supplementary materials.

## 4.3. Multi-view Recarving Strategy

Since our training data is sampled along a fixed direction and the directionality of Fourier Occupancy Fields, there are a few artifacts along the direction orthogonal to the normal direction of the generated shape. To tackle this issue while maintaining multi-views consistency, we propose the multi-view recarving strategy to eliminate artifacts at edges. Different from the resampling in Chupa [21], we perform this process on 3D space and fuse them by calculating the blending occupancy field.

In detail, for each sampling process, we first sample a Gaussian noise  $\tilde{z}_t \sim N(0, 1)$ . Then according to Eq. (4), we perform the complete denoising and decoding process to obtain the FOF  $C_{init}$  and occupancy field  $F_{init}$ . Based on the  $C_{init}$ , we can get the initial human mesh  $\mathcal{M}_{init}$ , which can have some artifacts in other views. To tackle these arti-

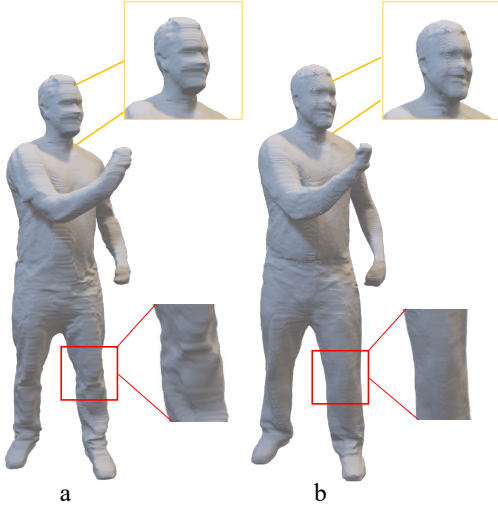


Figure 4. Ablation study on multi-view recarving strategy. With the multi-view recarving strategy (b), some artifacts can be avoided, compared with the variant without this strategy (a).

facts, we transform the yaw of the body  $\mathcal{M}_{init}$  orientation to get  $\mathcal{M}_\theta$ . After that, we turn the 3D mesh into FOF  $C_\theta$  by sampling along the current orientation. With the  $C_\theta$ , we do the same thing as Sec. 4.1: leveraging the encoder  $\mathcal{E}$  to get the latent code  $\hat{z}$ . After that, we re-execute the forward process of diffusion, adding a few steps of noise to  $\hat{z}$ . Then, we use the denoising model  $\epsilon_\theta$  to denoise the noisy  $\hat{z}$ . As before, we pass the denoised latent code through the decoder  $\mathcal{D}$  to get the FOF  $C_\theta$ . Meanwhile, we reconstruct the occupancy field  $F_\theta$  from FOF  $C_\theta$  by efficient Fourier inversion. At last, we blend the occupancy fields of different views and extract the 3D human mesh from the occupancy fields.

#### 4.4. High-frequency Enhancer

For efficient human representation and modeling of data distribution, we only save low-frequency terms while using the Fourier occupancy field for representation. However, some abandoned high-frequency information is also important for human shape details. Therefore, based on the generation of low-frequency FOF feature in Sec. 4.1, we propose the High-Frequency enhancer to recover these precise details, as shown in Fig. 2. In detail, we learn a reference-based decoding network  $\mathcal{D}_h$  based on the latent space and decoder from the auto-decoder claimed in Sec. 4.1 to produce high-frequency terms. To enhance the perception of latent-space contextual information, we introduce additional skip connections for each layer in  $\mathcal{D}_h$ , which is used to fuse the feature map from the relevant layers in the decoder  $\mathcal{D}_l$ . Then, we calculate the l2 loss between the predicted terms and high-frequency ground truth as the supervision to optimize  $\mathcal{D}_h$ . In this way, we achieve the map from the low-frequency domain to the high-frequency domain.

Table 2. Quantitative evaluation. We report two types of FID scores on the test dataset.

Method	FID <sub>normal</sub> ↓	FID <sub>shade</sub> ↓
Chupa <sub>coarse</sub>	51.60	73.03
Chupa <sub>fine</sub>	29.90	45.49
Ours <sub>coarse</sub>	37.67	59.45
Ours <sub>fine</sub>	<b>23.89</b>	<b>41.20</b>

## 5. Experiments

### 5.1. Experimental Setup

- **Datasets.** We trained our model with THuman 2.0 [46], THuman 3.0 [41], 2k2k [14] and about 1500 high-quality meshes from commercial datasets. To ensure a fair comparison, we deviated from Chupa [21]’s settings and opted for a third-party dataset CustomHumans [15] as our test set. We do this because the sota methods’ training code is not publicly available and some of the datasets they use are not publicly available. For the training stage, we first sample 32 successive different angles of FOF along the yaw axis of the rotating human body to generate FOF feature maps for the same mesh. After that, we obtain the joint points for each mesh and calculate the compact spherical embedding of the 3D joint with the same sampling process of FOF.
- **Baselines.** We compare our method with Chupa [21] and AG3D [9] as baselines. Chupa is the current state-of-the-art method for generating 3D human geometry. It can optimize the SMPL mesh by dual normal maps generated by the pose-guided diffusion model.
- **Metrics.** We measure the quality of the generated human mesh by using the Fréchet Inception Distance (FID) [2] between the rendering normal maps [6, 21] and shading images [21, 40] of the generated meshes.

### 5.2. Implementation Details

We use an EMA rate of 0.9999 for all experiments. For the training stage of the FOF autoencoder, we trained it for 3 days on 8 NVIDIA A100 GPUs, with a batch size of 32. To represent and generate a high-quality 3D human geometry, the channels  $N$  of the FOF feature maps need to be set to at least 32. However, it is very difficult to model high-dimensional and multi-channel data for diffusion models. To address this issue, following the latent diffusion model [38], we utilize an auto-encoder to compress the raw high-dimensional data space into a lower-dimensional latent space, which encodes each shape into a normal distribution. In detail, we adopted a VAE-like auto-encoder which contains the encoder  $\mathcal{E}$  and decoder  $\mathcal{D}$ . We present more details in the supplementary material.



Figure 5. Our method can generate various high-quality 3D humans.

### 5.3. Generated Results

Fig. 5 shows various generated results by our method. It can be seen that our method can generate high-quality 3D humans with global structure, local details, and high resolution. Benefiting from our proposed compact spherical embedding of 3D joints, we can flexibly generate high-quality 3D humans guided by poses. Fig. 6 shows more genera-

tion results guided by poses. Although we have fixed the pose, our model still performs well in the diversity of generation. It can generate humans with different identities and costumes.

### 5.4. Comparison

**Qualitative and Quantitative Results.** We compare our method with the latest human generative models Chupa [21]

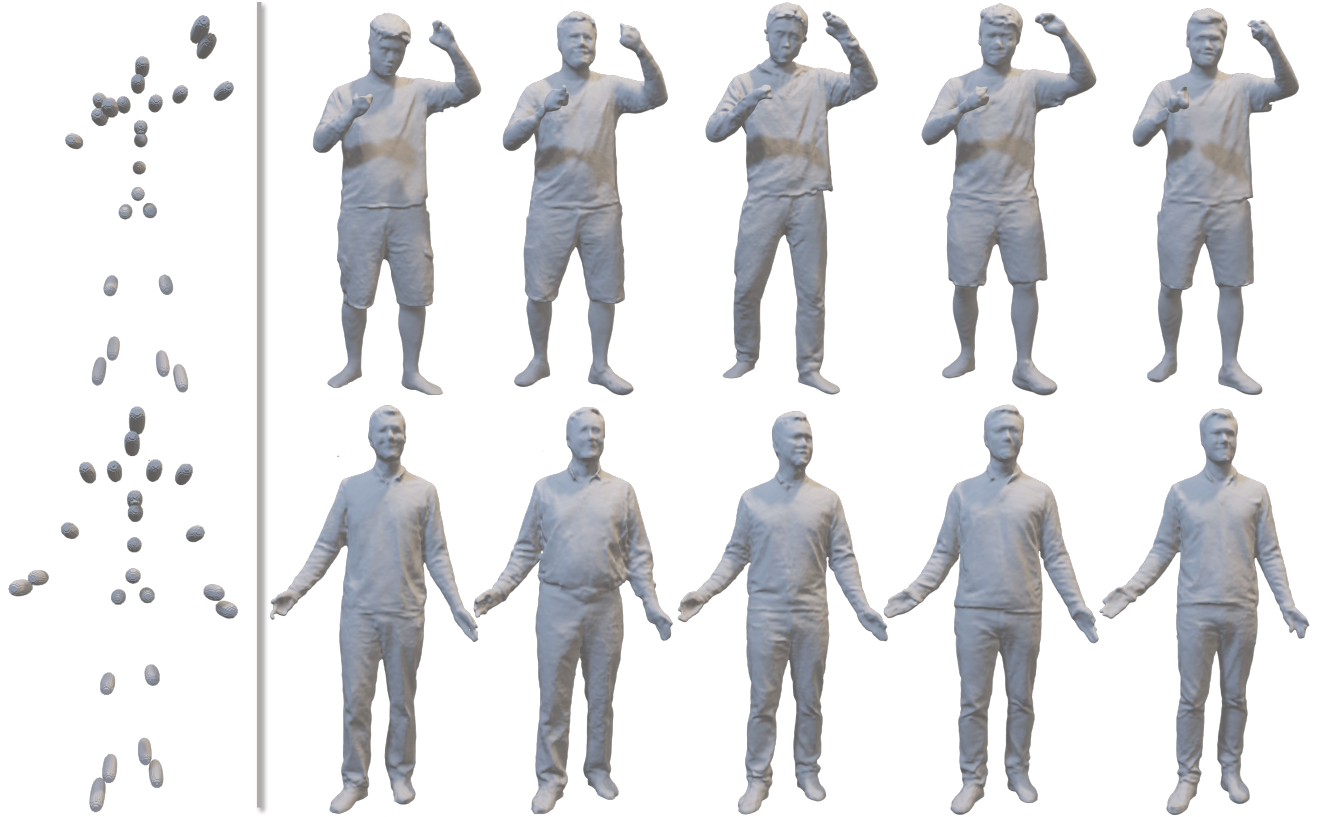


Figure 6. Our generated results guided by poses.

and AG3D [9]. In detail, We conduct a quantitative comparison experiment with Chupa to assess the quality of the generated meshes. Apart from this, we conduct a qualitative comparison experiment with AG3D and Chupa. To ensure a fair comparison, we try to control that the input poses of Chupa and our method are the same as much as possible. However, AG3D is not friendly to fixed poses as input, so we used random poses in the test stage. The quantitative results for human generation are shown in Tab. 2. Our method outperforms the current SOTA methods and achieves lower FID on both images. Fig. 7 shows qualitative comparison results, comparing the results generated by AG3D, our results have more details. Our results not only look more natural but also have better view consistency and superiority for modeling loose clothing when compared to the generated result of other methods. So our method can ensure the global structure and local details simultaneously.

**User Study.** To better evaluate our model, we conduct a perceptual study to ask the users about their preferences for the generated body geometry, choosing among our approach and two other current state-of-the-art methods, Chupa[21] and AG3D[9]. The results of the survey are shown in Tab. 3. In the user study, we collected 123 answers, including 54 females and 69 males with different

ages (6 users under 18, 113 users between 18 and 40, 2 users between 40 and 60, and 2 users above 60).

In the study, we show the human generation results of AG3D (Method A), Chupa (Method B), and our method (Method C) in video form. Our study is divided into two sections, with a total of 7 cases. In the first stage, cases 1 through 5 are responsible for studying individual generation performance (each case has three questions that are the same from case to case, 15 questions in total). The three questions are about generating a 3D human shape with 1. Global structure; 2. Local detail; and 3. Overall impression. Each user who participated in the survey was asked to rank the results shown in the video from best to worst according to these three metrics. Tab. 3 demonstrates that our approach is the most popular throughout the user study.

In the second stage, we focus mainly on the generative diversity of the different approaches. Since AG3D cannot support guidance by the human body pose, we only study the performance of methods B, and C in this section. Different from the first stage, we show the user multiple results in the form of images with two cases, both asking them which method is better for diversity. Each case includes 6 results for both methods. In this section, a total of 70.73% of the users consider the diversity of our methods to be superior to



Figure 7. The generated 3D humans compared with Chupa [21] and AG3D [9].

Chupa (Method B).

Table 3. Proportion of popularity of different methods in different metrics.

Method	AG3D(A)	Chupa(B)	Ours(C)
Global Structure	18.70%	32.20%	<b>49.10%</b>
Local Detail	18.05%	29.92%	<b>52.03%</b>
Overall Impression	19.02%	29.27%	<b>51.71%</b>
Diversity of Generation	-	29.27%	<b>70.73%</b>

### 5.5. Ablation Study

We have conducted extensive ablation studies to validate the components and settings of our pipeline. The quantitative comparisons use the same SMPL/pose guidance for evaluation. We also show and analyze different qualitative results to demonstrate the effectiveness of our module.

**Analysis on Different Pose-guided Strategy.** To validate the effectiveness of our pose-guidance, we train our model under different conditional information for pose-guidance.

There are three types of conditional information in our study, SMPL [26], joint (our compact spherical embedding of 3D joints), and IUUV [13]. We calculate the FID scores under the combination of different pose conditions. The results are shown in Tab. 4. According to the results, it can be inferred that the compact spherical embedding of 3D joints can generally improve the generation quality.

Table 4. Ablation study on different pose-guided strategy. We report FID scores for different combinations.

SMPL	Joints	IUV map	FID <sub>normal</sub> ↓
✓	✗	✗	49.16
✗	✓	✗	45.73
✗	✗	✓	39.51
✗	✓	✓	<b>38.40</b>

**Ablation on Multi-view Recarving Strategy and High-Frequency Enhancer.** The visual comparisons presented in

Fig. 4 demonstrate that the recarving strategy significantly enhances the local details of the generated human. To further measure the ability of other modules to capture local details, we carry out comparative experiments under different modules and calculate the FID scores. The results are shown in Tab. 5.

Table 5. Ablation study on multi-view recarving strategy and high-frequency enhancer. We report FID scores for different combinations.

Recarving Strategy	Enhancer	FID <sub>normal</sub> ↓
✗	✗	37.39
✓	✗	31.90
✗	✓	29.51
✓	✓	<b>25.67</b>

## 6. Conclusion and Discussion

**Conclusion.** In this paper, we introduce *Joint2Human*, a novel and efficient method for directly generating detailed 3D human geometry using 2D diffusion models. We propose a compact spherical embedding of 3D joints, for flexible control and utilizable human prior. We also design a high-frequency enhancer and a multi-view recarving strategy to seamlessly integrate the details from different views into a uniform global shape, and hence guarantee both global structure and local details. Besides, our method can also generate high-quality 3D humans guided by text. Experimental results demonstrate that our method outperforms the state-of-the-art methods, making it ideal for advanced 3D applications.

**Limitations.** Although our method can produce results with various poses, it’s still a huge challenge for it to support extreme poses, such as stooping down or standing on the head. More failure cases are shown in the supplementary material.

**Broader Impact.** Our method will promote the development of avatar generation, which is useful for VR/AR applications and makes up for the lack of 3D human datasets. However, this may also cause privacy and ethical problems. We suggest policymakers establish an efficient regulatory system and inform users about potential risks.

## References

- [1] Alexander W. Bergman, Petr Kellnhofer, Wang Yifan, Eric R. Chan, David B. Lindell, and Gordon Wetzstein. Generative neural articulated radiance fields. In *Adv. Neural Inform. Process. Syst.*, 2022. 2, 3
- [2] Naresh Bynagari. Gans trained by a two time-scale update rule converge to a local nash equilibrium. *Asian Journal of Applied Science and Engineering*, 8:25–34, 2019. 6
- [3] Yukang Cao, Yan-Pei Cao, Kai Han, Ying Shan, and Kwan-Yee K Wong. Dreamavatar: Text-and-shape guided 3d human avatar generation via diffusion models. *arXiv preprint arXiv:2304.00916*, 2023. 2, 3, 5
- [4] Eric R Chan, Connor Z Lin, Matthew A Chan, Koki Nagano, Boxiao Pan, Shalini De Mello, Orazio Gallo, Leonidas J Guibas, Jonathan Tremblay, Sameh Khamis, et al. Efficient geometry-aware 3d generative adversarial networks. In *IEEE Conf. Comput. Vis. Pattern Recog.*, 2022. 2, 3
- [5] Angel X Chang, Thomas Funkhouser, Leonidas Guibas, Pat Hanrahan, Qixing Huang, Zimo Li, Silvio Savarese, Manolis Sava, Shuran Song, Hao Su, et al. Shapenet: An information-rich 3d model repository. *arXiv preprint arXiv:1512.03012*, 2015. 3
- [6] Xu Chen, Tianjian Jiang, Jie Song, Jinlong Yang, Michael J Black, Andreas Geiger, and Otmar Hilliges. gdn: Towards generative detailed neural avatars. In *IEEE Conf. Comput. Vis. Pattern Recog.*, 2022. 2, 6
- [7] Yen-Chi Cheng, Hsin-Ying Lee, Sergey Tuyakov, Alex Schwing, and Liangyan Gui. SDFusion: Multimodal 3d shape completion, reconstruction, and generation. In *IEEE Conf. Comput. Vis. Pattern Recog.*, 2023. 3
- [8] Gene Chou, Yuval Bahat, and Felix Heide. Diffusion-sdf: Conditional generative modeling of signed distance functions. 2023. 3
- [9] Zijian Dong, Xu Chen, Jinlong Yang, Michael J Black, Otmar Hilliges, and Andreas Geiger. AG3D: Learning to Generate 3D Avatars from 2D Image Collections. In *Int. Conf. Comput. Vis.*, 2023. 2, 3, 5, 6, 8, 9
- [10] Qiao Feng, Yebin Liu, Yu-Kun Lai, Jingyu Yang, and Kun Li. Fof: Learning fourier occupancy field for monocular real-time human reconstruction. In *Adv. Neural Inform. Process. Syst.*, 2022. 3, 4
- [11] Jun Gao, Tianchang Shen, Zian Wang, Wenzheng Chen, Kangxue Yin, Daiqing Li, Or Litany, Zan Gojcic, and Sanja Fidler. Get3d: A generative model of high quality 3d textured shapes learned from images. In *Adv. Neural Inform. Process. Syst.*, 2022. 2
- [12] Ian Goodfellow, Jean Pouget-Abadie, Mehdi Mirza, Bing Xu, David Warde-Farley, Sherjil Ozair, Aaron Courville, and Yoshua Bengio. Generative adversarial nets. *Adv. Neural Inform. Process. Syst.*, 2014. 3
- [13] Riza Alp Güler, Natalia Neverova, and Iasonas Kokkinos. Densepose: Dense human pose estimation in the wild. In *IEEE Conf. Comput. Vis. Pattern Recog.*, 2018. 5, 9
- [14] Sang-Hun Han, Min-Gyu Park, Ju Hong Yoon, Ju-Mi Kang, Young-Jae Park, and Hae-Gon Jeon. High-fidelity 3d human digitization from single 2k resolution images. In *IEEE Conf. Comput. Vis. Pattern Recog.*, 2023. 6
- [15] Hsuan-I Ho, Lixin Xue, Jie Song, and Otmar Hilliges. Learning locally editable virtual humans. In *IEEE Conf. Comput. Vis. Pattern Recog.*, 2023. 6
- [16] Jonathan Ho, Ajay Jain, and Pieter Abbeel. Denoising diffusion probabilistic models. *Adv. Neural Inform. Process. Syst.*, 2020. 3, 4
- [17] Fangzhou Hong, Mingyuan Zhang, Liang Pan, Zhongang Cai, Lei Yang, and Ziwei Liu. Avatarclip: Zero-shot text-

- driven generation and animation of 3d avatars. *ACM Trans. Graph.*, 2022. 2, 3, 5
- [18] Fangzhou Hong, Zhaoxi Chen, Yushi LAN, Liang Pan, and Ziwei Liu. EVA3d: Compositional 3d human generation from 2d image collections. In *Int. Conf. Learn. Represent.*, 2023. 2, 3
- [19] Suyi Jiang, Haoran Jiang, Ziyu Wang, Haimin Luo, Wenzheng Chen, and Lan Xu. Humangen: Generating human radiance fields with explicit priors. In *IEEE Conf. Comput. Vis. Pattern Recog.*, 2023. 2, 3
- [20] Yuming Jiang, Shuai Yang, Haonan Qiu, Wayne Wu, Chen Change Loy, and Ziwei Liu. Text2human: Text-driven controllable human image generation. *ACM Trans. Graph.*, 2022. 5
- [21] Byungjun Kim, Patrick Kwon, Kwangho Lee, Myunggi Lee, Sookwan Han, Daesik Kim, and Hanbyul Joo. Chupa: Carving 3d clothed humans from skinned shape priors using 2d diffusion probabilistic models. *arXiv preprint arXiv:2305.11870*, 2023. 2, 3, 5, 6, 7, 8, 9
- [22] Nikos Kolotouros, Thiemo Alldieck, Andrei Zanfir, Eduard Gabriel Bazavan, Mihai Fieraru, and Cristian Sminchisescu. Dreamhuman: Animatable 3d avatars from text. 2023. 2, 3
- [23] Youngjoong Kwon, Dahun Kim, Duygu Ceylan, and Henry Fuchs. Neural human performer: Learning generalizable radiance fields for human performance rendering. *Adv. Neural Inform. Process. Syst.*, 2021. 2
- [24] Muheng Li, Yueqi Duan, Jie Zhou, and Jiwen Lu. Diffusion-sdf: Text-to-shape via voxelized diffusion. In *IEEE Conf. Comput. Vis. Pattern Recog.*, 2023. 3
- [25] Lingjie Liu, Marc Habermann, Viktor Rudnev, Kripasindhu Sarkar, Jiatao Gu, and Christian Theobalt. Neural actor: Neural free-view synthesis of human actors with pose control. *ACM Trans. Graph.*, 2021. 2
- [26] Matthew Loper, Naureen Mahmood, Javier Romero, Gerard Pons-Moll, and Michael J Black. SMPL: A skinned multi-person linear model. *ACM Trans. Graph.*, 2015. 2, 3, 5, 9
- [27] William E Lorensen and Harvey E Cline. Marching cubes: A high resolution 3d surface construction algorithm. In *Seminal graphics: pioneering efforts that shaped the field*, pages 347–353. 1998. 5
- [28] Ben Mildenhall, Pratul P. Srinivasan, Matthew Tancik, Jonathan T. Barron, Ravi Ramamoorthi, and Ren Ng. Nerf: Representing scenes as neural radiance fields for view synthesis. In *Eur. Conf. Comput. Vis.*, 2020. 2
- [29] Michael Niemeyer, Lars Mescheder, Michael Oechsle, and Andreas Geiger. Differentiable volumetric rendering: Learning implicit 3d representations without 3d supervision. In *IEEE Conf. Comput. Vis. Pattern Recog.*, 2020. 2
- [30] Atsuhiko Noguchi, Xiao Sun, Stephen Lin, and Tatsuya Harada. Neural articulated radiance field. In *Int. Conf. Comput. Vis.*, 2021. 2
- [31] Atsuhiko Noguchi, Xiao Sun, Stephen Lin, and Tatsuya Harada. Unsupervised learning of efficient geometry-aware neural articulated representations. In *Eur. Conf. Comput. Vis.*, 2022. 2, 3
- [32] Roy Or-El, Xuan Luo, Mengyi Shan, Eli Shechtman, Jeong Joon Park, and Ira Kemelmacher-Shlizerman. StyleSDF: High-Resolution 3D-Consistent Image and Geometry Generation. In *IEEE Conf. Comput. Vis. Pattern Recog.*, 2022. 2, 3
- [33] Jeong Joon Park, Peter Florence, Julian Straub, Richard Newcombe, and Steven Lovegrove. Deepsdf: Learning continuous signed distance functions for shape representation. In *IEEE Conf. Comput. Vis. Pattern Recog.*, 2019. 2
- [34] Georgios Pavlakos, Vasileios Choutas, Nima Ghorbani, Timo Bolkart, Ahmed A. A. Osman, Dimitrios Tzionas, and Michael J. Black. Expressive body capture: 3d hands, face, and body from a single image. In *IEEE Conf. Comput. Vis. Pattern Recog.*, 2019. 2, 3, 5
- [35] Sida Peng, Yuanqing Zhang, Yinghao Xu, Qianqian Wang, Qing Shuai, Hujun Bao, and Xiaowei Zhou. Neural body: Implicit neural representations with structured latent codes for novel view synthesis of dynamic humans. In *IEEE Conf. Comput. Vis. Pattern Recog.*, 2021. 2
- [36] Sida Peng, Chen Geng, Yuanqing Zhang, Yinghao Xu, Qianqian Wang, Qing Shuai, Xiaowei Zhou, and Hujun Bao. Implicit neural representations with structured latent codes for human body modeling. *IEEE Trans. Pattern Anal. Mach. Intell.*, 2023. 2
- [37] Alec Radford, Jong Wook Kim, Chris Hallacy, Aditya Ramesh, Gabriel Goh, Sandhini Agarwal, Girish Sastry, Amanda Askell, Pamela Mishkin, Jack Clark, et al. Learning transferable visual models from natural language supervision. 2021. 3
- [38] Robin Rombach, Andreas Blattmann, Dominik Lorenz, Patrick Esser, and Björn Ommer. High-resolution image synthesis with latent diffusion models. In *IEEE Conf. Comput. Vis. Pattern Recog.*, 2022. 4, 6
- [39] Olaf Ronneberger, Philipp Fischer, and Thomas Brox. U-net: Convolutional networks for biomedical image segmentation. In *Medical Image Computing and Computer-Assisted Intervention—MICCAI 2015: 18th International Conference, Munich, Germany, October 5-9, 2015, Proceedings, Part III 18*, pages 234–241. Springer, 2015. 3
- [40] Jessica Shue, Eric Chan, Ryan Po, Zachary Ankner, Jiajun Wu, and Gordon Wetzstein. 3d neural field generation using triplane diffusion. pages 20875–20886, 2022. 6
- [41] Zhaoqi Su, Tao Yu, Yangang Wang, and Yebin Liu. Deepcloth: Neural garment representation for shape and style editing. *IEEE Trans. Pattern Anal. Mach. Intell.*, 2023. 6
- [42] Tengfei Wang, Bo Zhang, Ting Zhang, Shuyang Gu, Jianmin Bao, Tadas Baltrusaitis, Jingjing Shen, Dong Chen, Fang Wen, Qifeng Chen, et al. Rodin: A generative model for sculpting 3d digital avatars using diffusion. In *IEEE Conf. Comput. Vis. Pattern Recog.*, 2023. 2, 3
- [43] Chung-Yi Weng, Brian Curless, Pratul P. Srinivasan, Jonathan T. Barron, and Ira Kemelmacher-Shlizerman. HumanNeRF: Free-viewpoint rendering of moving people from monocular video. In *IEEE Conf. Comput. Vis. Pattern Recog.*, 2022. 2
- [44] Zhangyang Xiong, Di Kang, Derong Jin, Weikai Chen, Linchao Bao, Shuguang Cui, and Xiaoguang Han. Get3dhuman:

- Lifting stylegan-human into a 3d generative model using pixel-aligned reconstruction priors. In *Int. Conf. Comput. Vis.*, 2023. [2](#), [3](#)
- [45] Kim Youwang, Kim Ji-Yeon, and Tae-Hyun Oh. Clip-actor: Text-driven recommendation and stylization for animating human meshes. In *Eur. Conf. Comput. Vis.*, 2022. [2](#), [3](#), [5](#)
- [46] Tao Yu, Zerong Zheng, Kaiwen Guo, Pengpeng Liu, Qionghai Dai, and Yebin Liu. Function4d: Real-time human volumetric capture from very sparse consumer rgb-d sensors. In *IEEE Conf. Comput. Vis. Pattern Recog.*, 2021. [6](#)
- [47] Jianfeng Zhang, Zihang Jiang, Dingdong Yang, Hongyi Xu, Yichun Shi, Guoxian Song, Zhongcong Xu, Xinchao Wang, and Jiashi Feng. Avatargen: a 3d generative model for animatable human avatars. In *Eur. Conf. Comput. Vis.*, 2022. [2](#), [3](#), [5](#)
- [48] Fuqiang Zhao, Wei Yang, Jiakai Zhang, Pei Lin, Yingliang Zhang, Jingyi Yu, and Lan Xu. Humannerf: Efficiently generated human radiance field from sparse inputs. In *IEEE Conf. Comput. Vis. Pattern Recog.*, 2022. [2](#)